Article

Spatial-Temporal Simulation of LAI on Basis of Rainfall and Growing Degree Days

Elham Davoodi [1], Hoda Ghasemieh [1,†], Okke Batelaan [2,†] [iD] and Khodayar Abdollahi [3,*,†] [iD]

[1] Faculty of Natural Resources and Earth Sciences, Kashan University, KM 6 BLVD. Ghotb Ravandi, Kashan 8731753153, Iran; Elhamdavoodi90@yahoo.com (E.D.); H.ghasemieh@kashanu.ac.ir (H.G.)

[2] National Centre for Groundwater Research and Training, College of Science and Engineering, Flinders University, Adelaide, SA 5042, Australia; okke.batelaan@flinders.edu.au

[3] Faculty of Natural Resources and Earth Sciences, Shahrekord University, BLVD. Rahbar, Shahrekord 8815648456, Iran

* Correspondence: kabdolla7@gmail.com; Tel.: +98-913-185-5688

† All authors contributed equally to this manuscript.

Abstract: The dimensionless Leaf Area Index (LAI) is widely used to characterize vegetation cover. With recent remote sensing developments LAI is available for large areas, although not continuous. However, in practice, continuous spatial-temporal LAI datasets are required for many environmental models. We investigate the relationship between LAI and climatic variable rainfall and Growing Degree Days (GDD) on the basis of data of a cold semi-arid region in Southwest Iran. For this purpose, monthly rainfall and temperature data were collected from ground stations between 2003 and 2015; LAI data were obtained from MODIS for the same period. The best relationship for predicting the monthly LAI values was selected from a set of single- and two-variable candidate models by considering their statistical goodness of fit (correlation coefficients, Nash-Sutcliffe coefficients, Root Mean Square Error and mean absolute error). Although various forms of linear and nonlinear relationships were tested, none showed a statistically meaningful relationship between LAI and rainfall for the study area. However, a two-variable nonlinear function was selected based on an iterative procedure linking rainfall and GDD to the expected LAI. By taking advantage of map algebra tools, this relationship can be used to predict missing LAI data for time series simulations. It is also concluded that the relationship between MODIS LAI and modeled LAI on basis of climatic variables shows a higher correlation for the wet season than for dry season.

Keywords: LAI estimation; growing degree days; rainfall; remote sensing; Behesht-Abad basin

1. Introduction

With progress in satellite Earth observation, remote sensing (RS) plays a major role in determining and monitoring the status of vegetation as by the use of Vegetation Indices (VI) [1,2]. VI is a type of multi-band spectral transformation with two or more reflective bands. These indices are designed to enhance the contribution of vegetation properties by providing more reliable spatial data about canopy structural variations and spatial-temporal inter-comparisons of terrestrial photosynthetic activities [3]. For instance, VI can be used to quantify vegetation cover, vigor and density [4–7].

From a practical perspective, one of the most important biophysical variables is Leaf Area Index (LAI). LAI represents the amount of one-sided leaf tissue per unit area of underlying ground surface [8–12]. LAI controls many physical and biological processes associated with plant, water, soil and energy fluxes [13]. It affects the soil-water balance via its control on the interception and transpiration [13–15] and therefore plays a critical role in natural systems and their ecophysiological, hydrological, ecological and meteorological processes [16,17].

In general, there are two main groups of LAI measurements: classical and modern methods. Classical methods involve direct and indirect measurements [18]; direct methods require an effort in collecting an optimal sample size, which involves destructive harvest techniques [18]. Indirect methods allow the inference of LAI from observations of another variable [18], different types of indirect methods are listed in Table 1. Modern methods employ mainly new technologies such as remote sensing to come up with different LAI products (Table 1).

Table 1. Summary of types of LAI measurement methods.

	Methods		LAI Measurements		Reference
Classic	Direct measurements		● Litterfall measurements ● Biomass harvesting		[8] [19]
	Indirect measurements	Contact measurements	● Inclined point quadrat ● Allometric techniques		[20]
		Optical measurements	● Hemispherical photography ● Plant Canopy Analyzer ● SunScan Ceptometer ● Airborne LiDAR		[19]
			● Hybrid method	● the neural network ● the lookup table	[20]
Modern	Using new technologies such as remote sensing		● MODIS ● CYCLOPES ● GLOBECARBON ● Geoland2 ● GLASS		[21]

Measuring the spatial and temporal variation of LAI is difficult [22]; however, this surface parameter can be derived using satellite optical imagery [16,22]. For large scale applications LAI products can e.g. be obtained from the Moderate Resolution Imaging Spectrometer (MODIS) with a global coverage. MODIS is a sun-synchronous orbit sensor residing aboard the Terra and Aqua remote sensing platforms, providing a view of the Earth's surface for every 1 to 2 days. The MODIS sensor is a multi-band sensor that collects remotely sensed data within 36 spectral bands, ranging in wavelengths from 0.4 μm to 14.4 μm. Its imagery products provide a series of bands with a nominal resolution of 250 m at nadir for two bands, 500 m resolution (5 bands), and 1 km for the rest of 29 bands [23]. Due to good validation and continuous updating, MODIS products are widely used for environmental modeling. Meanwhile, MODIS LAI product has received much attention for its long-term observation of land dynamics. Despite their significant temporal and spatial coverage, these satellite images are affected by cloud contamination or other atmospheric processes such as the influence of aerosols, which raises issues regarding the spatial-temporal continuity of the LAI data [24–28]. These data gaps limit the application of RS products for continuous modeling; a new method of data assimilation based on climatic variables could potentially resolve this issue. Hence, the goal of this study is to improve on the RS LAI data limitations by examining the predictive relationship between the climatic variables Growing Degree Days (GDD) and rainfall with LAI.

As an environmental factor, the effect of temperature on plant growth can be described by a thermal time concept. Since 1730 when Reaumur introduced the concept of heat units, or thermal time, many methods of calculating heat units have been used successfully in agricultural and natural resources sciences [29]. Particularly in the areas of crop phenology and development, the concept of heat units, measured in GDD, has vastly improved description and prediction of phenological events compared to other approaches such as time of year or number of days e.g., [30,31]. The heuristic indicator of GDD is calculated by summing up the positive daily differences between mean temperature and a baseline temperature [32,33]. GDD is a measurement unit that combines temperature and time such that the development duration of an organism's life cycle, or any stage or portion of the life cycle, decreases as the temperature increases [34] and describe the timing of biological processes [29,35]. Generally, GDD is used to include the temperature effects on the plant and describe the timing of

biological processes; it varies with growth stage [29,35]. It is the simplest model to account for the temperature effect on vegetative and reproductive development and has therefore some limitations for extreme high temperatures [36]. It allows for a rough estimation of the time at which a given growth phase is going to occur for a particular location [37].

Normalized Difference Vegetation Index (NDVI) is a RS indicator that is associated with LAI. Many studies present a correlation between rainfall and NDVI for different parts of the world [38–40]. Although a number of researchers such as [41] have indicated that no significant correlation could be established between rainfall and NDVI, Wang, Q. et al. [42] reported strong linear relationships during the leaf production and leaf senescence periods, but the relationship was found to be poor during periods of maximum LAI, due to the saturation of NDVI above certain LAI values.

So far, no study investigated the combined relationship among LAI, GDD and rainfall. This research is designed to establish a spatial-temporal LAI model based on the relationship between LAI, GDD and rainfall at the basin scale. The general objective of the study is to reduce embedded uncertainty in RS-based LAI data assimilation. Additionally, we construct a spatial mathematical relationship between LAI and rainfall/GDD, while also the temporal variation of the variables in the study area is investigated.

2. Materials and Methods

2.1. Study Area

The relationship between LAI and rainfall/GDD was investigated with example data from the Behesht-Abad Basin, which is the largest basin in Chaharmahal and Bakhtiari province, southwestern Iran (Figure 1). The basin drains an area of about 3860 km^2 to the Great Karoun drainage system, the largest river in the country. Topographically, Behesht-Abad Basin is located within the Zagros Mountains. The basin's elevation ranges from 1660 m up to 3620 m. It is characterized by a cold semi-arid climate and its temperature varies between 8.5 and 13.0 °C. The Behesht-Abad Basin receives an average annual rainfall of 322 mm [43].
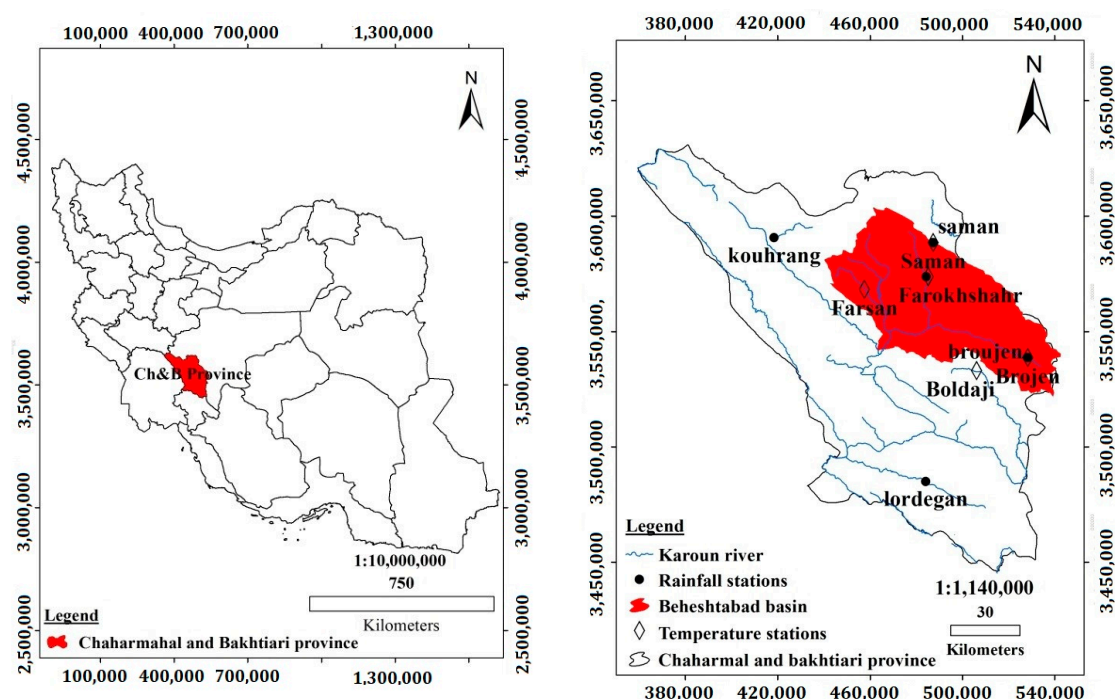
Figure 1. Left: Iran with the Chaharmahal and Bakhtiari province; **Right**: Behesht-Abad Basin boundary and the location of rainfall and temperature stations.

2.2. Data

In order to establish a model for simulating spatial-temporal LAI variability at basin scale, this study utilizes ground station monthly rainfall data, monthly T_{max} and T_{min} and remotely sensed LAI. The analysis is performed for 13 years from 2003 to 2015.

2.2.1. LAI Data

Currently the standard MODIS LAI products are provided at 500 m spatial resolution. These products include LAI retrievals from Terra MODIS, Aqua MODIS and combined Terra-Aqua MODIS sensors. The temporal compositing periods of provided data are 8 and 4 days [44]. There are various versions of MODIS products, but in this study we used MODIS collection 6 (MOD15A2H), which is an 8-day composite data set with 500 m pixel size. MOD15A2H and MOD15A2 are similar products in every aspect except for their spatial resolution, which is 500 m and 1000 m respectively. The data is based on an algorithm that chooses the best pixel available from all the acquisitions of the Terra sensor over an 8-day period. The archive of satellite data covers the time period from 2001 to present. LAI maps over the Behesht-Abad Basin were derived from the http://earthexplorer.usgs.gov/ web-site. The temporal resolutions of the images were up-scaled to a monthly time scale in order to match with rainfall and temperature data. Annual LAI maps for each year (2003 to 2015) were obtained through averaging, by aggregating monthly values.

The MODIS LAI values range between 0 and 255. Any pixel with a value more than 249 was set to "NO DATA" (Table 2), as there was no inland fresh water, sparse vegetation (rock, tundra, and desert), perennial snow, permanent wetlands or inundated marshlands in the study area. The spatial average of LAI for each month was determined. A simple bias correction based on monthly long-term factors was used so that LAI values follow the annual pattern of evapotranspiration calculated from OPTIWAT software [45] in the study area.

Table 2. LAI Fill value legend [44].

Value	Description
255	Filled value (when no reflectance or land cover value)
254	perennial salt or inland fresh water
253	barren, sparse vegetation (rock, tundra, desert)
252	perennial snow, ice
251	permanent wetlands/inundated marshlands
250	urban/built−up
249	unclassified or not able to determine

2.2.2. Rainfall Data

Monthly rainfall data for the period 2003–2015 was collected from five rain gauges in the Behesht-Abad Basin including Broojen, Kohrang, Lordegan, Saman and Shahrekord stations (Figure 1). Time series maps of monthly rainfall were obtained by Kriging and Weighted Least Square (WLS) interpolation methods. The monthly rainfall maps have a 500 m cell resolution and are geo-referenced with the LAI time series. Also the spatial average rainfall for each month was calculated.

2.2.3. Temperature Data

Mean monthly minimum and maximum temperature data is required for evaluating the Growing Degree Days (GDD) values. Recorded temperature for the same period as LAI and rainfall was collected from 5 ground stations in the Behesht-Abad Basin including Broojen, Farsan, Farrokhshar, Saman and Boldaji stations (Figure 1). GDD is defined as the daily difference between the average

of the daily T_{max} and T_{min} and the base temperature (T_{base}) that plants need for growth [29]. GDD is calculated as:

$$GDD = \left[\frac{(T_{max} + T_{min})}{2} \right] - T_{base} \tag{1}$$

T_{max} is daily maximum air temperature, T_{min} is daily minimum air temperature. T_{base} is the temperature below which the process of interest does not progress [29] and can vary based on species and there are several methods to estimate it. Because a temperature above 0 °C is considered the vegetation activation temperature; in this study T_{base} was assumed 0.4 °C.

Equation (1) assumes daily temperature data, here however we calculated GDD on basis of monthly T_{max}, T_{min} and T_{base} [36]. The assumption is that the mean monthly GDD on basis of monthly data is approximately equal to mean monthly GDD on basis of daily data. We tested this hypothesis from 2003 until 2015 and show that both monthly GDD estimates are in good agreement (Figure 2).
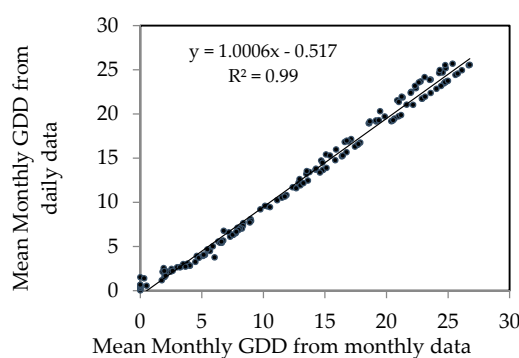
Figure 2. The relationship between mean monthly GDD from monthly data and mean monthly GDD from daily data.

2.3. Method

We tested various relationships between LAI-rainfall, LAI-GDD and LAI-rainfall-GDD by curve fitting; the fitted relationships are shown in Table 3.

Table 3. The tested relationships between LAI, rainfall (P) and GDD, a, b, c and d are parameters.

Model	Equation	LAI and Rainfall (X = Rainfall)					LAI and GDD (X = GDD)				
		a	b	c	d	R^2	a	b	c	d	R^2
MMF	$LAI = \frac{ab + cX^d}{b + X^d}$	1.31	2783.99	0.85	2.40	0.67	0.32	3.8	1.63	0.94	0.91
Exponential	$LAI = a(b - \exp(-cX))$	0.88	2.46	0		0.65	1.04	1.25	0.2		0.88
Linear	$LAI = bX + a$	1.31	−0.01			0.65	0.74	0.03			0.91
Quadratic	$LAI = a + bX + cP^2$	1.33	0	0		0.66	0.46	0.11	0		0.91
Rational	$LAI = \frac{a + bX}{1 + cX + dX^2}$	1.32	0	0.01	0	0.67	0.37	0.25	0.11	0	0.91
Harris	$LAI = \frac{1}{(a + bX^c)}$	0.75	0	0.88		0.67	3.37	−2.14	0.07		0.84

In order to better understand the relationship between LAI and rainfall a correlation analysis with Reconnaissance Drought Index (RDI) was performed. RDI is a relatively new index used for drought characterization based on a balance between precipitation and potential evapotranspiration (Thornthwaite method) [46]. Due to integration of both precipitation and evapotranspiration, the index is considered to be an influential indicator for drought assessment [47]. Three versions of RDI are easy and simple to calculate if monthly precipitation and PET are available: Initial RDI (RDI_0),

normalized RDI (RDI$_n$) and standardized RDI (RDI$_{st}$). Initial RDI may be calculated for each month, seasons (3-month, 4-month, etc.) or hydrological year. RDI$_0$ is defined as [47]:

$$\text{RDI}_0^{(i)} = \frac{\sum_{j=1}^{12} P_{ij}}{\sum_{j=1}^{12} \text{PET}_{ij}}, i = 1(1)N \text{ and } j = 1(1)12 \tag{2}$$

where P_{ij} and PET_{ij} respectively are the precipitation and potential evapotranspiration of the j month of the i-th hydrological year. In the study region the hydrological year runs from October to September. N is the total number of years of the available data time series. Then RDI$_n$ for each year is computed as

$$\text{RDI}_n^{(i)} = \frac{\text{RDI}_0^{(i)}}{\overline{\text{RDI}_0}} - 1 \tag{3}$$

where $\overline{\text{RDI}_0}$ is the arithmetic mean of RDI$_0$ values [34]. The computational approach for RDI$_{st}$, is similar in procedure to the SPI calculation (Equation (4)).

$$\text{RDI}_{st(k)}^{(i)} = \frac{y_k^{(i)} - \overline{y}_k}{\hat{\sigma}_{yk}} \tag{4}$$

where y_k is the ln(RDI$_0$), $\overline{y}_k$ is the arithmetic mean of all y_k, and $\hat{\sigma}_{yk}$ is its standard deviation.

2.4. Model Performance

Four evaluation metrics, Nash-Sutcliffe Coefficient (NS) (Equation (5)), coefficient of determination (R^2) (Equation (6)), Root Mean Square Error (RMSE) (Equation (7)) and mean absolute error (MAE) (Equation (8)) were used to quantify how well the fitted model can predict the LAI values based on climatic variables. By definition a NS value of 1 indicates a perfect fit between observed and modeled LAI values. In cases that there is no relationship between the simulated and remotely sensed LAI values then the NS coefficient is close to or less than 0. R^2 ranges from 0 to 1 with higher values indicating better agreement [23,48]. An R^2 of 1 indicates that the estimated LAI perfectly correlates with the LAI data. RMSE and MAE range from 0 to $+\infty$ with closer to zero indicating better agreement.

$$\text{NS} = 1 - \frac{\sum_{i=1}^{N}(S_i - O_i)^2}{\sum_{i=1}^{N}(O_i - \overline{O}_i)^2} \tag{5}$$

$$R^2 = 1 - \frac{\sum_{i-1}^{N}(O_i - S_i)^2}{\sum_{i-1}^{N}(O_i - \overline{O}_i)^2} \tag{6}$$

$$\text{RMSE} = \sqrt{\frac{1}{N}\sum_{i=1}^{N}(O_i - S_i)^2} \tag{7}$$

$$\text{MAE} = \frac{1}{N}\sum_{i=1}^{N}|O_i - S_i| \tag{8}$$

where O_i is observed values, S_i is the predicted value and $\overline{O}_i$ is the mean of the observations.

3. Results and Discussion

3.1. Relationship between LAI, GDD and Rainfall

In this study, to obtain a general relationship between LAI, rainfall and GDD, several empirical relationships were evaluated (Table 2). Long-term continuous linear regression analysis was carried out for the entire Behesht-Abad Basin on basis of the 13 years of available time series of rainfall,

GDD and LAI (Figure 3) [28]. The range for GDD was between 0 and 26 degrees, while for rainfall the range was very wide, between 0 and 186 mm. Visual interpretation of Figure 3 also shows that from 2003 until 2015 both LAI and GDD indicate a matching trend over time, especially during wet months. The relationship between rainfall and GDD was reversed compared to LAI-GDD. When GDD starts to increase from early April to early October, rainfall shows minimum value.

　　A minimum rainfall (0 mm) was reported for August (2003, 2006, 2007, 2008, 2011 and 2013) and September (2003, 2005, 2007, 2011, 2012, 2013 and 2014) while the rainfall in July and June is relatively low (Figure 3A). The highest recorded monthly rainfall was 186 mm for April 2004 (the average rainfall from 2003 to 2015 is 26.83 mm). Many researchers [30,41,49–51] have found a strong correlation between LAI and rainfall. However, here seasonal variation of rainfall demonstrates a substantially different seasonal pattern than LAI. Hence, despite testing six different relationships between LAI and rainfall (Table 2), all relationships demonstrated low R^2 values.
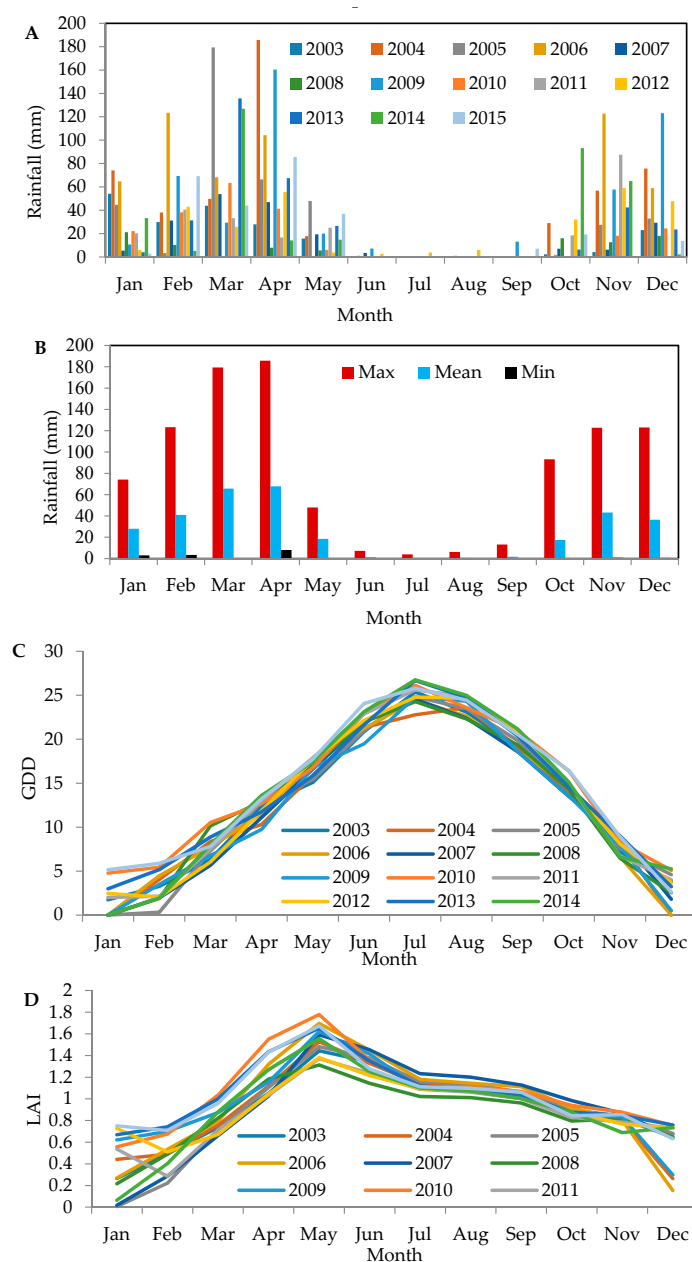
Figure 3. Spatially averaged time series of (**A**) monthly rainfall, (**B**) max, min and mean monthly rainfall, (**C**) monthly GDD and (**D**) monthly MODIS LAI.

The strong seasonal variation of GDD values shows an approximate similarity with the LAI values as it was expected. In response to environmental variables, LAI increases at the beginning of the year until mid-May after which it decreases until it reaches a minimum value in December (Figure 3D). This seasonal pattern is observed during the whole study period. The highest LAI value in the study area was 1.77 and the lowest value 0.005; the average LAI from 2003 to 2015 was 0.94. GDD factor increase at beginning of the year until it reaches to a maximum during mid-July, and then it starts to decrease until the end of December (Figure 3C). The highest GDD value for the region was 26.75 and the lowest value 0; the average GDD from 2003 to 2015 was 13.09.

GDD values are consistent with LAI for the period 2003 till 2015 in the study area (Figure 3C,D). On the one hand the basin is characterized by cold weather on other hand plant growth is strongly dependent on temperature during the growing season with each species having specific temperature requirements. Both rainfall and GDD have a contribution in temporal and spatial variability of LAI. The LAI increases with the rainfall and GDD, thus models based on GDD and rainfall (Table 3) (Equations (9) and (10)) are tested to simulate the dynamic changes in LAI over the studied period.

$$LAI = a\left(P_{Kriging}\right)^b e^{\frac{-(GDD-c)^2}{d}} \qquad (9)$$

$$LAI = a\left(P_{WLS}\right)^b e^{\frac{-(GDD-c)^2}{d}} \qquad (10)$$

where P is the spatially interpolated (Kriging or WLS) rainfall, a, b, c and d are model parameters to be estimated via calibration. To determine the effect of rainfall and GDD on the simulated LAI, a sensitivity analysis was performed (Figure 4). It showed that GDD has a greater impact on the simulated LAI than rainfall.
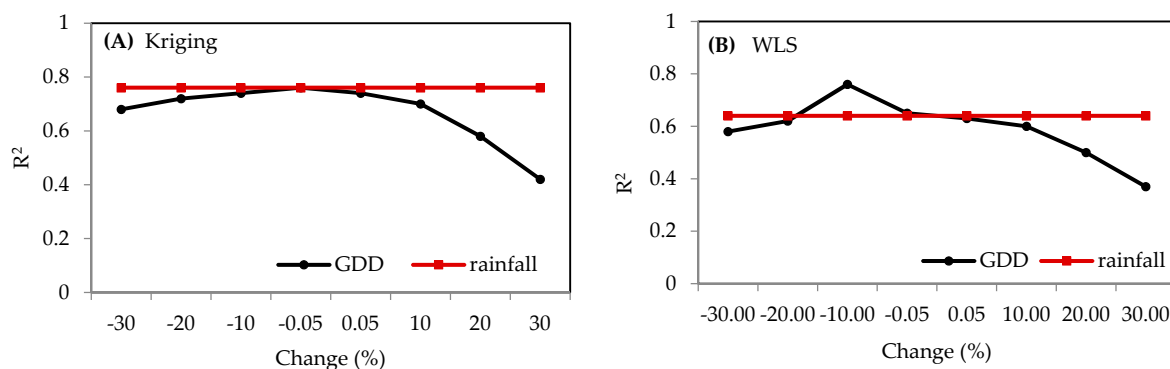

Figure 4. The result of sensitivity analyses of rainfall (Kriging (**A**) vs. WLS (**B**)) and GDD.

Model calibration and validation are both critical steps in any model application. For this purpose, MODIS LAI and simulated LAI time series are split into two separate periods [52]. 70% from 2003 to 2011 is used for model calibration and the rest (from 2011 to 2015) for validation. The results of model calibration are shown in Table 4.
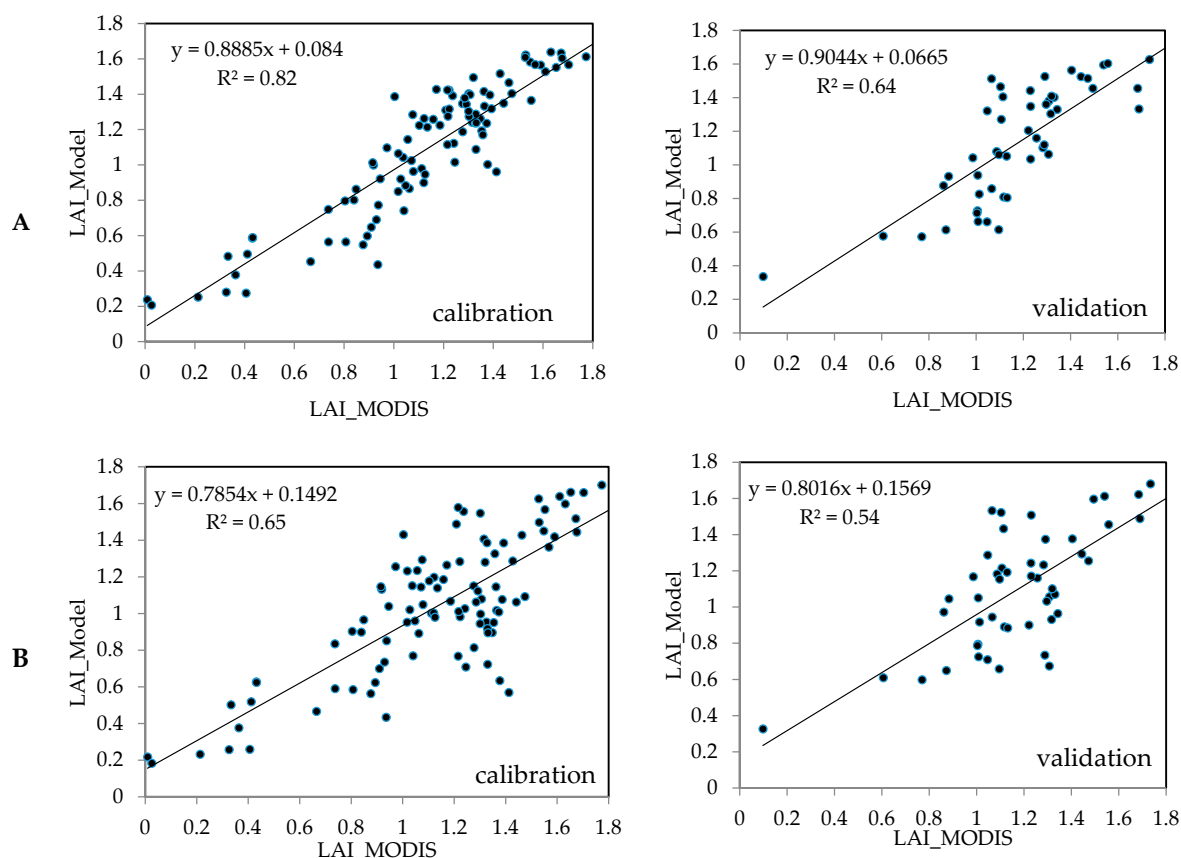
Table 4. Results of calibration and validation.

Method/Parameter	a	b	c	d	Calibration				Validation			
					R^2	NS	RMSE	MAE	R^2	NS	RMSE	MAE
Kriging	1.4	0.04	19	310	0.82	0.80	0.16	0.13	0.64	0.51	0.21	0.17
WLS	1.25	0.08	16	225	0.65	0.56	0.25	0.20	0.54	0.35	0.24	0.20

The models of Equations (9) and (10) showed respectively a performance for the calibration of R^2 = 0.82 and 0.65, NS = 0.80 and 0.56, RMSE = 0.16 and 0.25, MAE = 0.13 and 0.20, while the validation

values are respectively R^2 = 0.64 and 0.54, NS = 0.51 and 0.31, RMSE = 0.21 and 0.24, MAE = 0.17 and 0.20 (Figure 5). These results indicated for Equations (9) and (10) respectively a good and satisfactory model performance for both the calibration and validation.


Figure 5. Calibration and validation of MODIS LAI and simulated LAI time series, (**A**) Results based on Equation (9) model; (**B**) Results based on Equation (10) model.

The time series of the simulated LAI and MODIS LAI are presented in Figure 6. It shows except for some moments (black circles in Figure 6) that both time series follow a very similar pattern. To some extent the mismatch between simulated and MODIS LAI may be related to the resolution of the MODIS images.

The method of interpolation of the rainfall has an impact on the model performance. Figure 7 shows that the R^2, NS, RMSE and MAE coefficient between MODIS LAI and LAI model with Kriging interpolation of the rainfall is respectively 0.77 (with 95% confidence level), 0.74, 0.18 and 0.14, while for the LAI model with WLS interpolation of rainfall the equivalent performance values are 0.62 (with 95% confidence level), 0.51, 0.25 and 0.20. These performance results confirm that the simulated LAI on basis of a combination GDD and rainfall data simulate well the MODIS LAI. Figure 7 shows that model has a relatively low accuracy in estimating LAI in low range and conversely. The models overestimate in the 0.6 to 0.8 range and underestimate in the 1.4 to 1.6 range.

Also, the relationship between MODIS LAI and monthly simulated LAI was evaluated with R^2, NS, RMSE and MAE criteria (Table 5). In both methods (Kriging and WLS) the highest R^2 values were obtained for December, January and February (last month of the fall and two months in winter time) and lowest value in July, August, September and November (during summer months). During December till February the maximum value of rainfall and the minimum value of GDD within the region occur (Figure 3), while during July till September the minimum value of rainfall and the maximum value of GDD occur. The highest RMSE values were obtained in January, October and

December with kriging method and during summer months with WLS method. Similar results were obtained for MAE. The highest RMSE and MAE values indicate that model performance is low in the summer months.
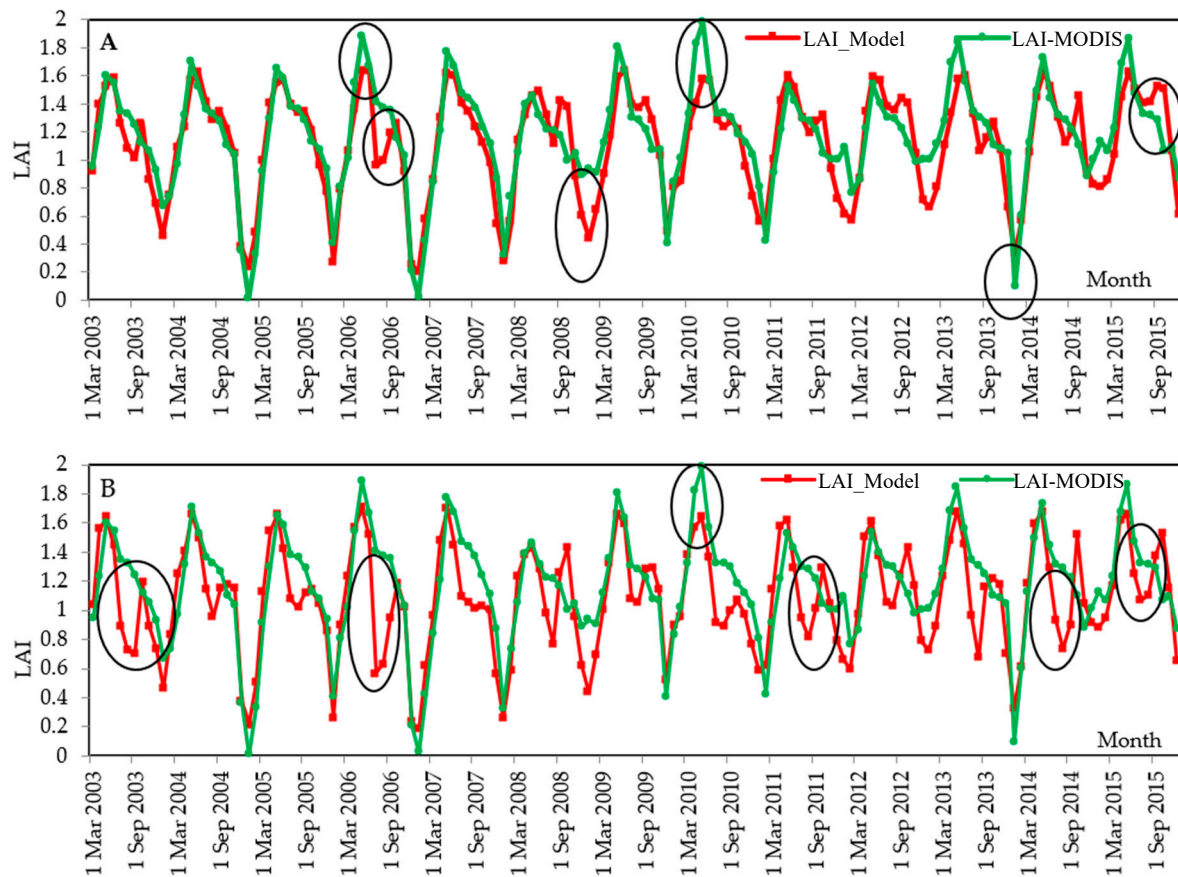
Figure 6. Time series of the spatially-averaged MODIS LAI vs. simulated LAI, (**A**) LAI model Equation (9) with rainfall interpolated with Kriging; (**B**) LAI model Equation (10) with rainfall interpolated with WLS.
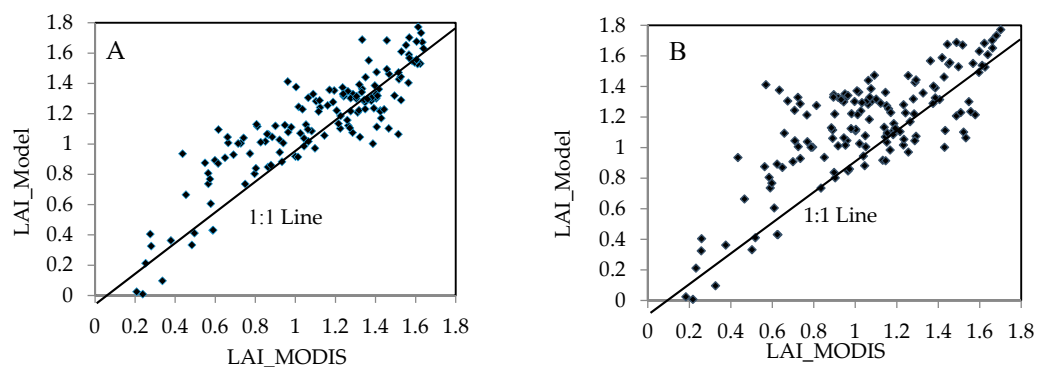
Figure 7. The scatter plots of spatially-averaged MODIS LAI vs. (**A**) LAI_Model with Kriging interpolation of Rainfall; (**B**) LAI_Model with WLS interpolation of Rainfall.

Table 5. Monthly R^2, NS, RMSE and MAE values for the years 2003 till 2015 for simulated LAI (**top**: Equation (9), **bottom**: Equation (10)) vs. MODIS LAI.

	Month	R^2	NS	RMSE	MAE	Month	R^2	NS	RMSE	MAE
Kriging	January	0.74	0.50	0.28	0.24	July	0.02	−4.62	0.13	0.08
	February	0.68	0.48	0.17	0.15	August	0.03	−8.52	0.16	0.13
	March	0.44	0.42	0.11	0.09	September	0.04	−7.32	0.15	0.13
	April	0.08	−0.04	0.20	0.17	October	0.43	−16.33	0.24	0.21
	May	0.30	−0.62	0.19	0.16	November	0.03	−2.14	0.10	0.08
	June	0.68	0.34	0.08	0.06	December	0.84	0.20	0.24	0.22
	Month	R^2	**NS**	**RMSE**	**MAE**	**Month**	R^2	**NS**	**RMSE**	**MAE**
WLS	January	0.72	0.57	0.26	0.22	July	0.01	−44.88	0.39	0.36
	February	0.64	0.60	0.15	0.14	August	0.05	−76.85	0.46	0.43
	March	0.42	−0.04	0.15	0.13	September	0.04	−21.96	0.26	0.21
	April	0.08	−0.12	0.21	0.17	October	0.51	−18.36	0.25	0.20
	May	0.41	0.09	0.14	0.11	November	0.006	−2.35	0.11	0.09
	June	0.57	−0.89	0.14	0.12	December	0.81	0.42	0.20	0.18

3.2. Annual Analysis

Annual and seasonal changes in LAI values, in response to change in GDD and rainfall are clearly noticed in Figures 6 and 7. The temporal charts at monthly scale (Figure 8) show a large variability in LAI, GDD and rainfall over the study period. Maximum LAI values are observed in May, while the maximum GDD values are observed in July. On the other hand, the wet months with a peak in rainfall are March, April and November. Generally, values of LAI were very low in January, February and December. Lowest GDD values occur in January, February and December, while lowest rainfall occurs in June, July, August and September. A concurrency in the minimum values of both LAI and GDD during the months of in January, February and December is noticed. Figure 8 shows that approximately with two or three months delay, LAI values for this basin responds to rainfall. That means for each month that rainfall is high, an increased LAI can be seen after two or three months. However, the range of monthly changes during 2003 to 2015 for LAI was only between 0.005 and 1.77.

The RDI index was calculated (Figure 9a) and lag time effects on the relationship between drought conditions and LAI are presented in Table 6. Figure 9b shows that the impact of drought on LAI appears after a 3-month delay (R^2 = 0.51).

Table 6. Correlation coefficients between LAI and RDI after applying a lag time.

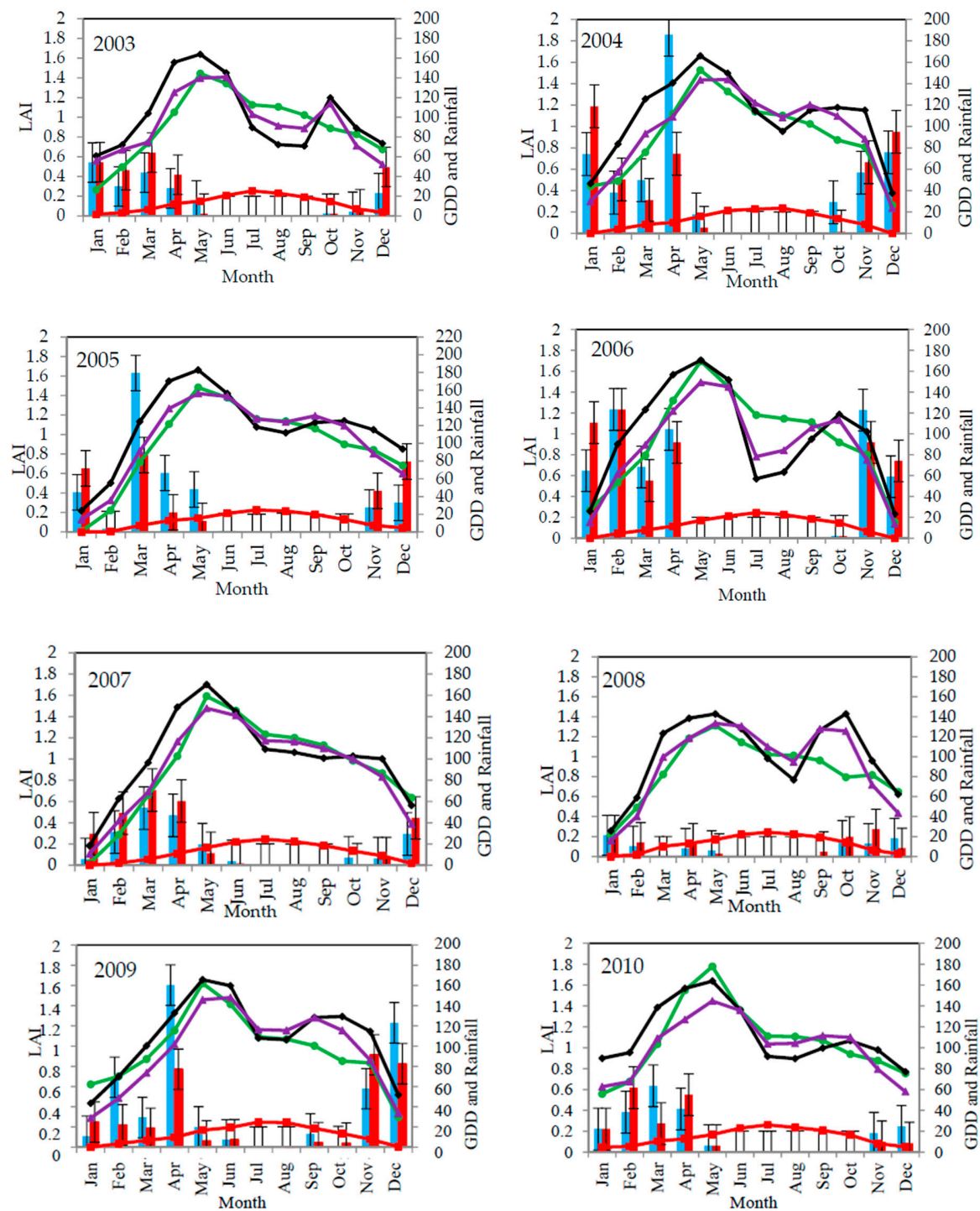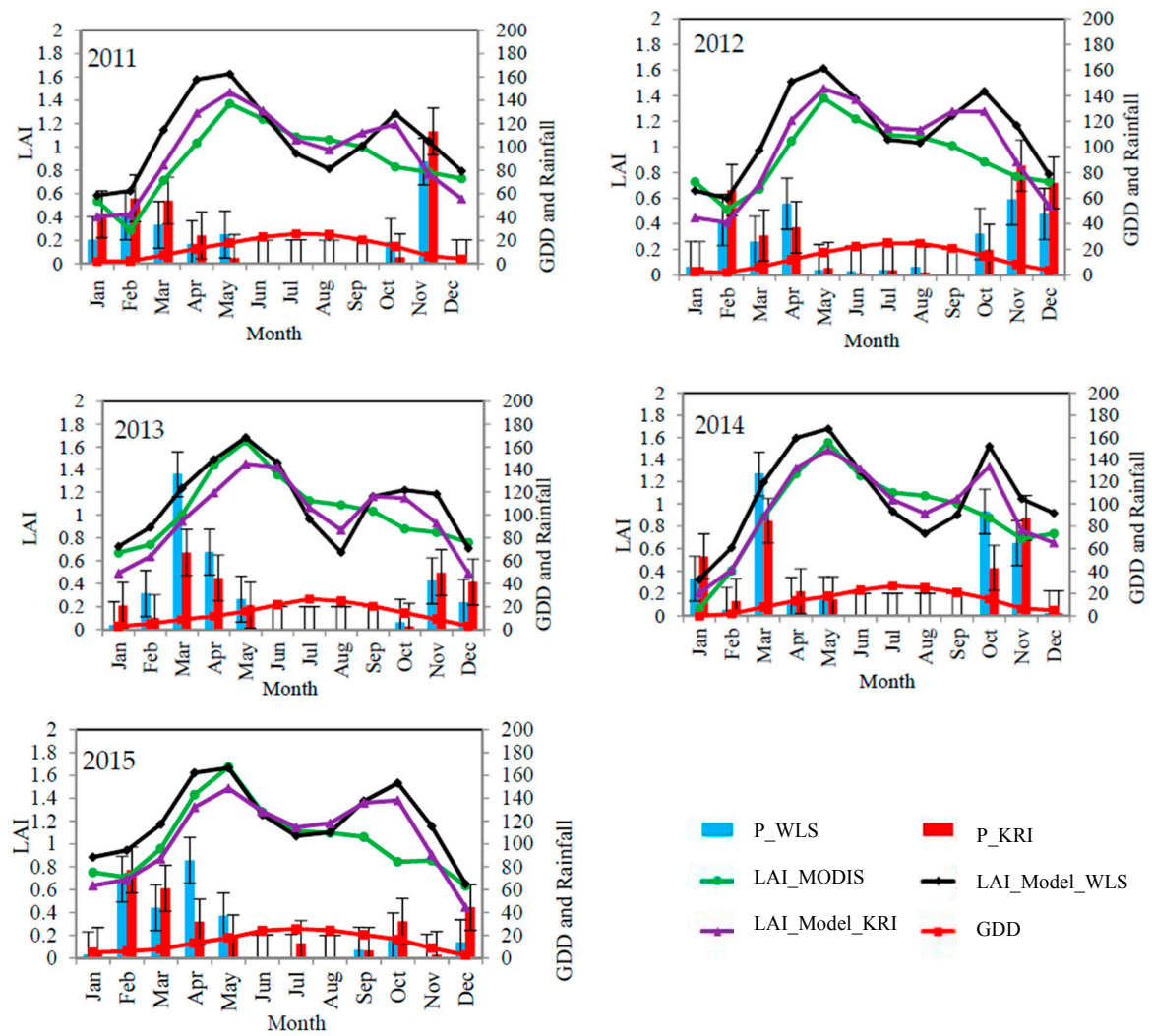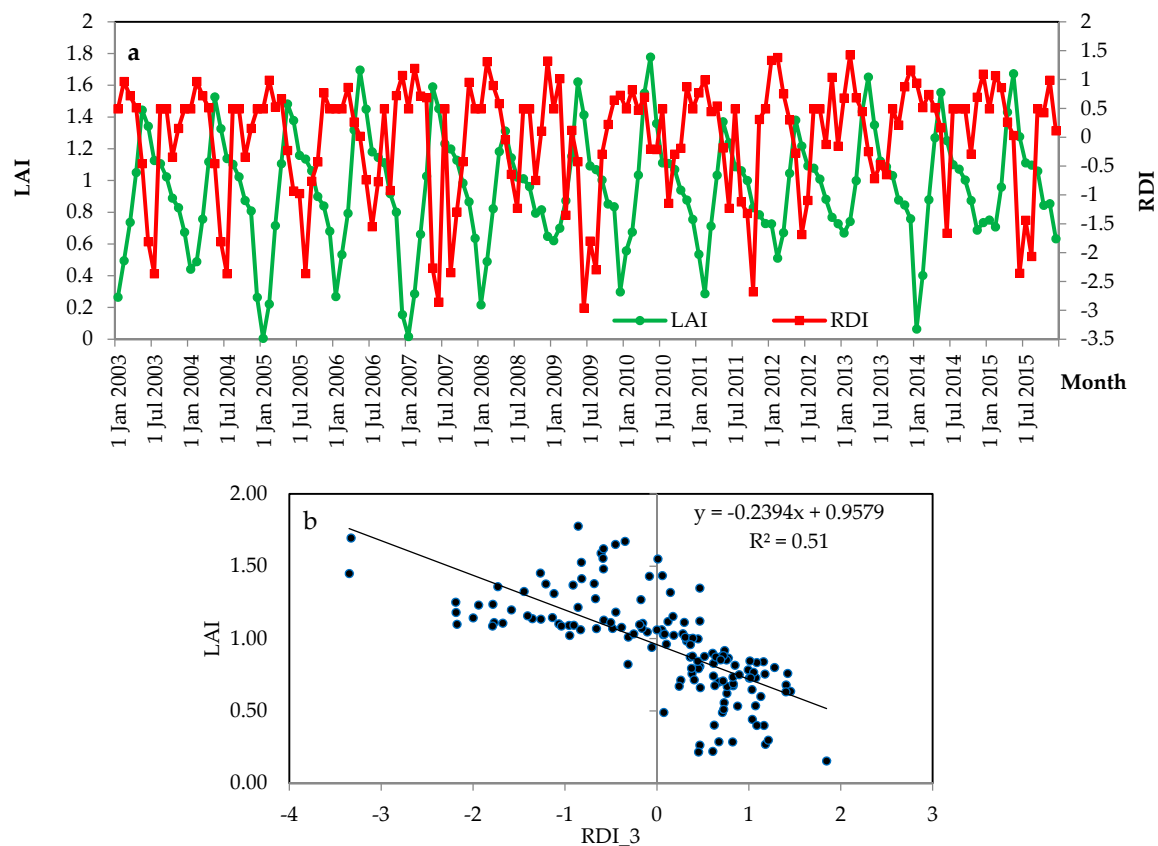| Lag Time	R^2	Lag Time	R^2
0	0.24	12	0
3	0.51	18	0.17
6	0.27	24	0
9	0	48	0

Figure 8. *Cont.*

Figure 8. Monthly values for MODIS LAI, simulated LAI (using GDD and Kriging or WLS), rainfall (Kriging, WLS) and GDD for the years 2003 till 2015.

Figure 9. (**a**) RDI and LAI values for Behesht-Abad Basin (2003 to 2015), (**b**) Correlation coefficient between LAI and RDI with a 3-month lag time.

4. Conclusions

Considering that climate change is happening, it is important to understand how vegetation responds to changing environmental factors. In this paper, we analyzed the response of LAI to climatic variables at basin scale. A spatial-temporal data set comprising thirteen years of monthly LAI, rainfall and GDD for a cold semi-arid area has been analyzed for this purpose. Results indicate that LAI development is mainly affected by GDD and 3 months of delayed rainfall. The main conclusions of this research are:

(1) Despite testing six different relationships between LAI and rainfall at basin scale, none of the relationships were successful for this study area. Similarly, the seven tested functions between LAI and GDD failed to provide an acceptable fit.

(2) The relationship between a combination of GDD and rainfall with LAI shows a high model efficiency for both calibration and validation stages.

(3) The form of the fitted model indicates that the relationship between LAI and rainfall/GDD is non-linear.

(4) The relationship between MODIS LAI and simulated LAI on basis of climatic variables (rainfall and GDD) shows a higher correlation in months with no water stress.

RS-based LAI maps are generally available but they are conditioned by several technical and environmental factors. This results in missing LAI values in the time series, which limits hydrological modeling with continuous time series of LAI maps. This study provides a framework for producing consistent estimates of LAI values based on routine climatic variables to fill the missing values.

Author Contributions: All co-authors of this manuscript significantly contributed to different phases of this manuscript including the preparation, analysis, review and editing. They contributed equally to this work.

Conflicts of Interest: The authors declare no conflict of interest.

References

1. Sivakumar, M.V.; Roy, P.S.; Harmsen, K.; Saha, S.K. Satellite remote sensing and GIS applications in agricultural meteorology. In Proceedings of the Training Workshop, Dehra Dun, India, 7–11 July 2003; Available online: https://pdfs.semanticscholar.org/7b88/85cccf8810290237e3a2a3893f8fc83e89f3.pdf (accessed on 21 November 2017).
2. Jonckheere, I.; Fleck, S.; Nackaerts, K.; Muys, B.; Coppin, P.; Weiss, M.; Baret, F. Review of methods for in situ leaf area index determination, Part I. Theories, sensors and hemispherical photography. *Agric. For. Meteorol.* **2004**, *121*, 19–35. [CrossRef]
3. Huete, A.; Didan, K.; Miura, T.; Rodriguez, E.P.; Gao, X.; Ferreira, L.G. Overview of the radiometric and biophysical performance of the MODIS vegetation indices. *Remote Sens. Environ.* **2002**, *83*, 195–213. [CrossRef]
4. Hansen, M.C.; Defries, R.S.; Townshend, J.R.G.; Sohlberg, R. Global land cover classification at 1 km spatial resolution using a classification tree approach. *Int. J. Remote Sens.* **2000**, *21*, 1331–1364. [CrossRef]
5. Lawley, V.; Lewis, M.; Clarke, K.; Ostendorf, B. Site-based and remote sensing methods for monitoring indicators of vegetation condition: An Australian review. *Ecol. Indic.* **2016**, *60*, 1273–1283. [CrossRef]
6. Loveland, T.R.; Reed, B.C.; Brown, J.F.; Ohlen, D.O.; Zhu, Z.; Yang, L.; Merchant, J.W. Development of a global land cover characteristics database and IGBP DISCover from 1 km AVHRR data. *Int. J. Remote Sens.* **2000**, *21*, 1303–1330. [CrossRef]
7. Southworth, J.; Munroe, D.; Nagendra, H. Land cover change and landscape fragmentation–comparing the utility of continuous and discrete analyses for a western Honduras region. *Agric. Ecosyst. Environ.* **2004**, *101*, 185–205. [CrossRef]
8. Breda, N.J.J. Ground-based measurements of leaf area index: A review of methods, instruments and current controversies. *J. Exp. Bot.* **2003**, *54*, 2403–2417. [CrossRef] [PubMed]
9. Chen, J.M.; Cihlar, J. Retrieving Leaf Area Index for Boreal Conifer Forests using Landsat TM Images. *Remote Sens. Environ.* **1996**, *55*, 153–162. [CrossRef]
10. Monteith, J.L.; Unsworth, M.H. *Principles of Environmental Physics*, 2nd ed.; Arnold, E., Ed.; Butterworth-Heinemann: London, UK, 1990; p. 291. ISBN 0-7131-2931-X.
11. Myneni, R.B.; Nemani, R.R.; Running, S.W. Estimation of Global Leaf Area Index and Absorbed PAR using Radiative Transfer Models. *IEEE Trans. Geosci. Remote Sens.* **1997**, *35*, 1380–1393. [CrossRef]
12. Watson, D.J. Comparative physiological studies on the growth of field crops: I. Variation in net assimilation rate and leaf area between species and varieties, and within and between years. *Ann. Bot.* **1947**, *11*, 41–76. [CrossRef]
13. Chen, M.; Willgoose, G.R.; Saco, P.M. Investigating the Impact of Leaf Area Index Temporal Variability on Soil Moisture Predictions using Remote Sensing Vegetation Data. *J. Hydrol.* **2015**, *522*, 274–284. [CrossRef]
14. Albertson, J.D.; Kiely, G. On the structure of soil moisture time series in the context of land surface models. *J. Hydrol.* **2001**, *243*, 101–119. [CrossRef]
15. Piayda, A.; Dubbert, M.; Werner, C.; Correia, A.V.; Pereira, J.S.; Cuntz, M. Influence of woody tissue and leaf clumping on vertically resolved leaf area index and angular gap probability estimates. *For. Ecol. Manag.* **2015**, *340*, 103–113. [CrossRef]
16. Cao, X.L.; Zhou, Z.H.; Chen, X.D.; Shao, W.W.; Wang, Z.R. Improving leaf area index simulation of IBIS model and its effect on water carbon and energy—A case study in Changbai Mountain broadleaved forest of China. *Ecol. Model.* **2015**, *303*, 97–104. [CrossRef]
17. Ishihara, M.I.; Hiura, T. Modeling leaf area index from litter collection and tree data in a deciduous broadleaf forest. *Agric. For. Meteorol.* **2011**, *151*, 1016–1022. [CrossRef]
18. Campos-Taberner, M.; García-Haro, F.J.; Confalonieri, R.; Martínez, B.; Moreno, Á.; Sánchez-Ruiz, S.; Gilabert, M.A.; Camacho, F.; Boschetti, M.; Busetto, L. Multitemporal Monitoring of Plant Area Index in the Valencia Rice District with PocketLAI. *Remote Sens.* **2016**, *8*, 202. [CrossRef]

19. Fleck, S.; Raspe, S.; Cater, M.; Schleppi, P.; Ukonmaanaho, L.; Greve, M.; Hertel, C.; Weis, W.; Rumpf, S. Leaf Area Measurments; Manual Part XVII. In *Manual on Methods and Criteria for Harmonized Sampling, Assessment, Monitoring and Analysis of the Effects of Air Pollution on Forests*; UNECE ICP Forest Programme Co-Ordinating Center: Hamburg, Germany, 2012; p. 37. Available online: http://www.icp-forest.org/Manual.htm (accessed on 21 November 2017).

20. Jensen, J.R. *Remote Sensing of the Environment—An Earth Resource Perspective*, 2nd ed.; Pearson Prentice Hall: Upper Saddle River, NJ, USA, 2007; pp. 382–392. ISBN 978-0131889507.

21. Liang, S.; Zhang, X.; Xiao, Z.; Cheng, J.; Liu, Q.; Zhao, X. *Global Land Surface Satellite (GLASS) Products, Algorithms, Validation and Analysis*; Springer Science & Business Media: Berlin, Germany, 2014.

22. Chen, J.M.; Deng, F.; Chen, M. Locally Adjusted Cubic-Spline Capping for Reconstructing Seasonal Trajectories of a Satellite-Derived Surface Parameter. *IEEE Trans. Geosci. Remote Sens.* **2006**, *44*, 2230–2238. [CrossRef]

23. Legates, D.R.; McCabe, G.J. Evaluating the use of "goodness-of-fit" Measures in hydrologic and hydroclimatic model validation. *Water Resour. Res.* **1999**, *35*, 233–241. [CrossRef]

24. Borak, J.S.; Jasinski, M.F. Effective interpolation of incomplete satellite-derived leaf area index time series for the continental United States. *Agric. For. Meteorol.* **2009**, *149*, 320–332. [CrossRef]

25. Fang, H.; Liang, S.; Townshend, J.R.; Dickinson, R.E. Spatially and temporally continuous LAI data sets based on an integrated filtering method: Examples from North America. *Remote Sens. Environ.* **2008**, *112*, 75–93. [CrossRef]

26. Gao, F.; Morisette, J.T.; Wolfe, R.E.; Ederer, G.; Pedelty, J.; Masuoka, E.; Myneni, R.; Tan, B.; Nightingale, J. An algorithm to produce temporally and spatially continuous MODIS-LAI time series. *Geosci. Remote Sens. Lett.* **2008**, *5*, 60–64. [CrossRef]

27. Lawrence, P.J.; Chase, T.N. Representing a new MODIS consistent land surface in the Community Land Model (CLM 3.0). *J. Geophys. Res. Atmos.* **2007**, *112*, G01023. [CrossRef]

28. Potithep, S.; Nasahara, N.K.; Muraoka, H.; Nagai, S.; Suzuki, R. What is the actual relationship between LAI and VI in a deciduous broadleaf forest? In Proceedings of the International Archives of the Photogrammetry. Remote Sensing and Spatial Information Science, Kyoto, Japan, 9–12 August 2010; Volume 38, pp. 609–614.

29. McMaster, G.S.; Wilhelm, W. Growing degree-days: One equation, two interpretations. *Agric. For. Meteorol.* **1997**, *87*, 291–300. [CrossRef]

30. Cross, H.Z.; Zuber, M.S. Prediction of flowering dates in maize based on different methods of estimating thermal units. *Agron. J.* **1972**, *64*, 351–355. [CrossRef]

31. McMaster, G.S.; Smika, D.E. Estimation and evaluation of winter wheat phenology in the central Great Plains. *Agric. For. Meteorol.* **1988**, *43*, 1–18. [CrossRef]

32. Gallagher, J.N. Field studies of cereal leaf growth: I. Initiation and expansion in relation to temperature and ontogeny. *J. Exp. Bot.* **1979**, *117*, 625–636. [CrossRef]

33. Ruml, M.; Vukovic, A.; Milatovic, D. Evaluation of different methods for determining growing degree-day thresholds in apricot cultivars. *Int. J. Biometeorol.* **2010**, *54*, 411–422. [CrossRef] [PubMed]

34. Salazar-Gutierrez, M.R.; Johnson, J.; Chaves-Cordoba, B.; Hoogenboom, G. Relationship of base temperature to development of winter wheat. *Int. J. Plant Prod.* **2013**, *7*, 741–762.

35. Baker, D.G.; Sharratt, B.S.; Chiang, H.C.; Zandlo, J.A.; Ruschy, D.L. Base temperature selection for the prediction of European corn borer instars by the growing degree day method. *Agric. For. Meteorol.* **1984**, *32*, 55–60. [CrossRef]

36. Salama, M.A.; Yousef, K.M.; Mostafa, A.Z. Simple equation for estimating actual evapotranspiration using heat units for wheat in arid regions. *J. Radiat. Res. Appl. Sci.* **2015**, *8*, 418–427. [CrossRef]

37. Fischer, R.A.; Aguilar, I.; Maurer, R.; Rivas, S. Density and row spacing effects on irrigated short wheat at low latitude. *J. Agric. Sci.* **1976**, *87*, 137–147. [CrossRef]

38. Groeneveld, D.P.; Baugh, W.M. Correcting satellite data to detect vegetation signal for eco-hydrologic analyses. *J. Hydrol.* **2007**, *344*, 135–145. [CrossRef]

39. Kawabata, A.; Ichii, K.; Yamaguchi, Y. Global monitoring of interannual changes in vegetation activities using NDVI and its relationships to temperature and precipitation. *Int. J. Remote Sens.* **2001**, *2*, 1377–1382. [CrossRef]

40. Phu La, H.; Patrick, T.R.; Park, B.W.; Eo, Y.D. Analysis of the Relationship between MODIS NDVI, LAI and Rainfall in the Forest Region of Rwanda. *Int. J. Digit. Content Technol. Appl.* **2013**, *7*, 559–569. [CrossRef]

41. Onema, J.M.K.; Taigbenu, A. NDVI–rainfall relationship in the Semliki watershed of the equatorial Nile. *Phys. Chem. Earth* **2009**, *34*, 711–721. [CrossRef]

42. Wang, Q.; Adiku, S.; Tenhunen, J.; Granier, A. On the relationship of NDVI with leaf area index in a deciduous forest site. *Remote Sens. Environ.* **2005**, *94*, 244–255. [CrossRef]

43. Saeedinia, M.; Samadi, H.; Maleki, A.; Izadi, A. Evaluation of drought effect on groundwater resource and agricultural development in the Behesht Abad basin using WEAP model. *J. Water Soil Conserv.* **2011**, *18*, 17–36. (In Persian)

44. MODIS Web. Available online: https://modis.gsfc.nasa.gov/data/dataprod/mod15.php (accessed on 21 November 2017).

45. Alizadeh, A.; Kamali, G. *Crops Water Requirements in Iran*, 2nd ed.; Emam Reza University: Mashhad, Iran, 2009; pp. 50–200. ISBN 964-6582-76-1.

46. Tsakiris, G.; Vangelis, H. Establishing a drought index incorporating evapotranspiration. *Eur. Water* **2005**, *9*, 3–11.

47. Tsakiris, G.; Pangalou, D.; Vangelis, H. Regional drought assessment based on the reconnaissance drought index (RDI). *Water Resour. Manag.* **2007**, *21*, 821–833. [CrossRef]

48. Su, L.; Wang, Q.; Wang, C.; Shan, Y. Simulation Models of Leaf Area Index and Yield for Cotton Grown with Different Soil Conditioners. *PLoS ONE* **2015**, *10*, 1–19. [CrossRef] [PubMed]

49. Anderson, M.C.; Zolin, C.A.; Hain, C.R.; Semmens, K.; Yilmaz, M.T.; Gao, F. Comparison of satellite-derived LAI and precipitation anomalies over Brazil with a thermal infrared-based Evaporative Stress Index for 2003–2013. *J. Hydrol.* **2015**, *526*, 287–302. [CrossRef]

50. Camberlin, P.; Martiny, N.; Philippon, N.; Richard, Y. Determinants of the interannual relationships between remote sensed photosynthetic activity and rainfall in tropical Africa. *Remote Sens. Environ.* **2007**, *106*, 199–216. [CrossRef]

51. Udelhoven, T.; Stellmes, M.; Del Barrio, G.; Hill, J. Assessment of rainfall and NDVI anomalies in Spain (1989–1999) using distributed lag models. *Int. J. Remote Sens.* **2009**, *30*, 1961–1976. [CrossRef]

52. Klemes, V. Operational testing of hydrological simulation models. *Hydrol. Sci. J.* **1986**, *31*, 13–24. [CrossRef]